Monthly Notices of the ROYAL ASTRONOMICAL SOCIETY

MNRAS **521,** 3699–3707 (2023) https://doi.org/10.1093/mnras/stad662
Advance Access publication 2023 March 3

A search for chemical anomalies of seven A-type stars

Yahya Nasolo ★ and Seyma Çalışkan
Department of Astronomy and Space Sciences, Ankara University, Tandoğan, Ankara 06100, Turkey

Accepted 2023 February 25. Received 2023 February 25; in original form 2022 November 29

ABSTRACT

We present a chemical abundance analysis of seven A-type stars with no detailed chemical abundance measurements in the literature. High-resolution spectra of the targets – HD 2924, HD 4321, HD 26553, HD 125658, HD 137928, HD 154713, and HD 159834 – were obtained using the Coudé Echelle Spectrograph at the TÜBİTAK National Observatory. We determined the atmospheric abundances of the samples and measured the elemental abundances of C, N, O, Na, Mg, Al, Si, S, K, Ca, Sc, Ti, V, Cr, Mn, Fe, Co, Ni, Cu, Zn, Sr, Y, Zr, Ba, La, Ce, Nd, Sm, Eu, and Gd. The masses of the stars were estimated based on their evolutionary tracks, and their ages were calculated using isochrones. We also calculated the radii of the stars. The abundance patterns of HD 4321, HD 125658, and HD 154713 were found to be in agreement with those of classical Am stars, with underabundant Ca and Sc, overabundant heavier elements, and moderate overabundance of iron-peak elements. We found that HD 137928 and HD 159834 have abundance characteristics similar to marginal Am-type stars. The elemental distributions of HD 2924 and HD 26553 are consistent with the pattern of normal A-type stars. The iron, nickel, and zinc abundances of HD 125658 and HD 137928 are significantly higher than those of other Am stars. These values suggest that they are among the most metal-rich Am stars.

Key words: stars: abundances – stars: chemically peculiar – techniques: spectroscopic – instrumentation: spectrographs.

1 INTRODUCTION

In the course of stellar evolution, stars inherit the chemical composition of their birthplace; however, the atmospheric chemical abundance distribution changes over time due to poorly understood internal stellar processes. The warmer post zero-age main sequence (ZAMS) mid-massive stars, corresponding to mid-B to early-F spectral types, attract particular attention, since a substantial fraction exhibit chemical abundance anomalies, which reflect these internal processes. Detailed chemical abundance analysis of these stars is essential, since it potentially provides a basis for understanding such phenomena. Chemically peculiar (CP) metallic-line (Am) stars are the typical targets for these studies. CP stars are characterized by enhanced absorption lines (Preston 1974; Monier 2019). Am stars are A- to early F-type stars sharing the same region as normal A-type stars, with effective temperature ($T_{\rm eff}$) between 7000 and 9000 K. They lie in the cooler portion of main-sequence CP stars. Am stars were first recognized as a group by Titus & Morgan (1940). Preston (1974) classified CP stars into four groups, with Am stars being the CP1 group. Am stars are characterized by three spectral characteristics: the strength of their Balmer lines; their Ca II K lines, which are weaker than those of normal A-type stars with the same temperature; and their enhanced metallic lines relative to their normal counterparts. In typical Am star spectra, the intensity of the Ca II K line is weaker than that of the Balmer lines and resembles an earlier spectral type. The metallic lines are more intense and resemble a later spectral type (Roman, Morgan & Eggen 1948). Abt & Morgan (1976) stated that the Ca II K line in the spectra of such stars resembles the spectral type at least five subtypes earlier. Am stars with Ca II K and metallic lines differing by less than five subtypes are referred to as marginal Am stars (Trust et al. 2021). Underabundance of Sc II and/or Ca II is a discovery criterion for this class (Michaud, Alecian & Richer 2015). Based on observational statistics, the majority of Am stars are slow rotators (Fossati et al. 2008). This supports the hypothesis of chemical separation due to radiative diffusion and gravitational settling, since slow rotation is expected not to destroy the separation phenomenon (Michaud et al. 2015). Chemical separation requires calm atmospheres, which are expected given the slow rotation of these stars (Takeda et al. 2008; Fossati et al. 2008; Abt 2009). In close binaries, slow rotation is associated with tidal synchronization (Khokhlova 1981). However, observations of low-rotating normal A-type stars pose a challenge to this view of the impact of rotation. Normal A-type stars exhibit nearly solar abundances, with the heavier elements falling within the range of ±0.40 dex relative to the Sun (Adelman & Unsuree 2007). This work focuses on determining the chemical abundances and fundamental parameters (e.g. effective temperatures and surface gravities) of the sample stars in detail. The work is organized as follows: Section 2 describes the target selection, observations, and data reduction. We present the determination of atmospheric stellar parameters and the procedure used to perform the abundance analysis in Section 3. The evolutionary status of the stars is shown by employing the Hertzsprung–Russell (HR) diagram in Section 4. We discuss the results in Section 5 and we conclude in Section 6.

2 OBSERVATION DATA

2.1 Target selection

One of the dominant mixing processes that suppresses the effect of chemical separation in atomic diffusion is linked to rotational velocity. A statistical analysis of observations suggests that all

★ E-mail: nasolo@ankara.edu.tr

© The Author(s) 2023.
Published by Oxford University Press on behalf of Royal Astronomical Society. This is an Open Access article distributed under the terms of the Creative Commons Attribution License (http://creativecommons.org/licenses/by/4.0/), which permits unrestricted reuse, distribution, and reproduction in any medium, provided the original work is properly cited.

Downloaded from https://academic.oup.com/mnras/article/521/3/3699/7069350 by ANKARA UNIVERSITY user on 04 June 2023

Table 1. The observation log of the target stars. The *V*-band magnitudes were estimated by Oja (1991).

Star name	*V* mag (mag)	Exposure time (s)	Observation time (JD)	SNR (@5000–7000 Å)
HD 2924	6.700 [0.009]	4500 ×2	2457676.37750	297
HD 4321	6.510 [0.009]	4500 × 2	2457675.50366	250
HD 26553	6.080 [0.009]	4500 × 2	2455554.33347	287
HD 125658	6.445 [0.010]	4500 × 1	2458232.38508	115
HD 137928	6.430 [0.010]	4500 × 2	2458233.33802	280
HD 154713	6.441 [0.010]	4500 × 2	2458234.41497	302
HD 159834	6.100 [0.010]	4500 × 2	2458232.51027	362

main-sequence stars of the targeted temperature regime with equatorial rotational velocities less than 80 km s^{-1} are Am /Fm stars (Abt 2000). Abt & Moyd (1973) initially reported that the equatorial velocity of observed CP1 stars is less than 120 km s^{-1}. This observation is consistent with chemical separation due to atomic diffusion occurring when the He II convection zone disappears at equatorial velocities lower than 70−120 km s^{-1} (Michaud 1982). We therefore selected targets in this temperature regime with low rotation velocities ($v \sin i < 70$ km s^{-1}) and chemical abundances that have not been derived previously.

2.2 Observations and data reduction

For this study, we used the high-resolution $R \sim 40\,000$ spectroscopic data obtained by the Coudé Echelle Spectrograph attached to the 1.5-m Russian–Turkish Telescope (RTT-150) at TÜBİTAK National Observatory (TUG). The spectra cover a wavelength range of 3900–8770 Å. Along with the target star's spectra, each observation run began with acquiring calibration frames and arc spectra: the halogen lamp for flat-fielding and the Th–Ar lamp for wavelength calibration. Table 1 lists the observation log of our targets, including observation times, exposure times, numbers of co-added spectra, and signal-to-noise ratios (SNR). The raw spectra were reduced using IRAF's standard reduction routines. Initially, image header information was methodized to allow processing in the IRAF environment. The reduction process started with bias subtraction followed by flat-fielding. The next step was the removal of scattered light from star spectra. Using the Th–Ar spectra, we conducted wavelength calibration and lastly performed cosmic-ray removal. We measured the Doppler shift of the spectra using unblended moderately strong absorption lines. Then the heliocentric radial velocities ($V_{\rm helio}$) were determined and necessary Doppler corrections were applied to all spectra. For six of the targets, we acquired two spectral frames, which were combined to improve the SNR. We could not acquire a second frame for HD 125658 due to adverse weather. The echelle orders of the spectra were normalized according to spline-fitted continuum points. Fig. 1 shows a sample of normalized orders of the spectra of stars at about 5100 Å , as well as some of the identified unblended lines used for chemical abundance determination. The lines clearly exhibit the broadening effect of rotational velocity.

3 ATMOSPHERE PARAMETERS AND CHEMICAL ABUNDANCES

Spectroscopy and photometry are the traditional methods used to determine stellar atmospheric parameters. In this work, we employed both methods. We used the photometric method to find the initial atmospheric parameters, then we refined the parameters with the spectroscopic method.

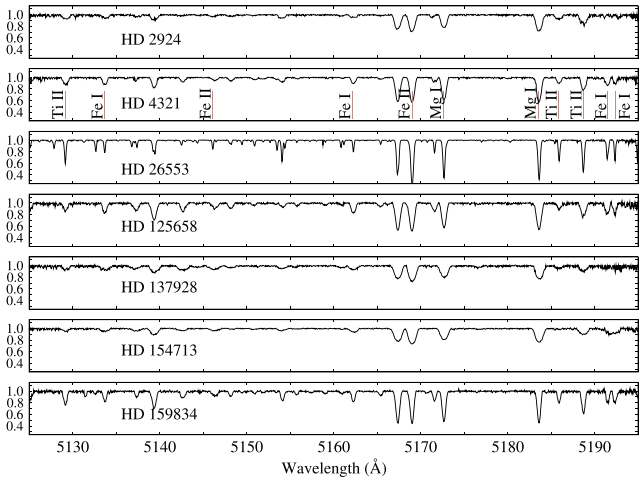


Figure 1. A sample of normalized orders of the target stars and some of the identified unblended lines used for chemical abundance determination.

3.1 Line identification and equivalent-width measurement

We used line lists from the Kurucz line database (Kurucz & Bell 1995) and the Vienna Atomic Line Database (Piskunov et al. 1995; Kupka et al. 1999; Ryabchikova et al. 1999). Line identification and equivalent-width measurements of the atomic species found in the spectra of the target stars were implemented through an Interactive Data Language (IDL) visualization program, BINMAG6 (Kochukhov 2018). Equivalent-width measurements were performed by Gaussian profile fitting of the lines. Table 2 lists the spectral lines measured.

3.2 Stellar parameters

Photometric stellar parameters were determined using the Strömgren *ubvyβ* photometric indices of Paunzen (2015). The photometric data were used in the calibrations performed by Napiwotzki, Schoenberner & Wenske (1993) to determine the $T_{\rm eff}$ and surface gravity (log *g*) of each target. These calibrations have systematic and statistical errors of 200 K for $T_{\rm eff}$ and 0.10 dex for log *g* (Napiwotzki et al. 1993). The computed stellar parameters are given in Table 3.

Spectroscopic atmospheric parameters determination: One of the classic methods used to yield the effective temperature spectroscopically is to employ Fe I lines throughout the stellar spectrum and iterate the effective temperature until their abundances show no trend with the excitation potential (EP) of each line. In contrast with photometric methods, no reddening information is needed for this technique; however, high-resolution spectra with a resolving power of $R \sim \lambda/\Delta\lambda \geq 15\,000$ are required, preferably with wide wavelength coverage throughout the optical range (Frebel et al. 2013). The different methods are known to produce temperatures with systematic

Downloaded from https://academic.oup.com/mnras/article/521/3/3699/7069350 by ANKARA UNIVERSITY user on 04 June 2023

Table 2. List of spectral lines used in the abundance analysis of target stars. The full table is available online. A portion of the table is shown here.

Atomic sp.	Wavelength (nm)	log *gf*	Equivalent width (pm) HD 2924	HD 4321	HD 26553	HD 125658	HD 137928	HD 154713	HD 159834
C I	477.0027	−2.722	...	...	...	...	...	...	01.50
C I	477.1742	−2.120	...	06.46	...	05.87	02.93	03.78	04.22
C I	477.5897	−2.163	02.98	05.38	01.60	03.09	...	...	...
C I	493.2049	−1.884	04.45	06.89	03.04	03.56	...	02.74	02.90
C I	502.3849	−2.400	...	02.25	00.71	...	...	...	02.02

Table 3. Photometrically determined stellar parameters.

Star name	$T_{\rm eff}$ [K]	log g [dex]
HD 2924	8633	3.45
HD 4321	7659	3.27
HD 26553	7783	2.41
HD 125658	7966	3.94
HD 137928	8382	3.81
HD 154713	8217	3.63
HD 159834	7799	3.57

offsets from each other. We used the photometrically determined atmospheric parameters ($T_{\rm eff}$, log g) to construct initial model atmospheres used in the EP method, where $T_{\rm eff}$ was derived from the excitation equilibrium of the Fe I lines. The models were constructed using ATLAS9 (Kurucz 1993a). Depending on the $T_{\rm eff}$ derived from the EP method, we derived the stellar surface gravities through Fe I–II ionization equilibrium. The log g value was determined from the balance of abundances derived from individual Fe I–II while the value of log g was iterated. The microturbulent velocity (ξ) was calculated by adopting the values that produced no trend of equivalent widths with abundances derived from individual Fe I lines. This allowed the chemical abundance of iron to be derived. We measured the v sin i of the target stars by comparing the observed spectra with the synthetic spectra. The synthetic spectra were produced using SYNTHE (Kurucz 2005b, 1993b). All atmospheric parameters derived from spectroscopy are listed in Table 4.

3.3 Abundance analysis

We derived the abundance of each atomic species using the measured equivalent widths in WIDTH9 (Kurucz 2005a; Sbordone et al. 2004), which uses ATLAS9 model atmospheres to compute line formation in local thermodynamic equilibrium. We avoided using lines of equivalent widths greater than 200 mÅ for the abundance analysis to avoid the use of saturated lines, which bias the abundances. We included hyperfine structure (HFS) splitting for the V, Sc, Mn, Y, and Ba spectral lines. HFS split lines occur due to electromagnetic multipole interaction between the nucleus and electrons, which arises from the energy of the nuclear magnetic dipole moment interacting with the magnetic field generated by the electrons and shifts the lines of different isotopes. HFS has a small broadening effect, shifting the lines and altering their shape, which may lead to erroneous interpretations of spectra with the equivalent-width method.

To measure the abundance of HFS elements, we generated synthetic spectra using SYNTHE (Kurucz 1993b, 2005b) with HFS line lists from the Kurucz database and fitted them with the observed spectra lines. The spectra generation includes broadening effects due to the instrumental profile and turbulent velocity. The abundance of the best fit between the observed and synthetic spectrum was adopted. The elemental abundances have random (σ_r) and systematic errors. The random errors are from the standard deviations of individual measurements. The systematic error of the chemical abundances due to atmosphere parameters is

$$\sigma_{\rm sys}=\sqrt{\sigma^2_{T\rm eff}+\sigma^2_{\log g}+\sigma^2_{\xi}}. \quad (1)$$

The total error is

$$\sigma_{\rm tot}=\sqrt[3]{\sigma^2_{\rm sys}+\sigma^2_r}/\sqrt{N}, \quad (2)$$

where N is the number of lines used to derive the chemical abundances. We present the elemental abundances along with the number of lines and their total errors in Tables 5 and 6. The solar abundance (log $\epsilon_{\odot}$) values are taken from Grevesse & Sauval (1998). Figs 2, 3, and 4 show the differences from solar abundances with total error bars. The abundance patterns of HD 4321, HD 125658, and HD 154713 show an agreement with the abundance patterns of classical Am stars, with underabundant Ca and Sc, overabundant heavier elements, and moderate overabundance of iron-peak elements. We compared these patterns with the classical Am HD 33266 studied by Çalışkan et al. (2015). We find that HD 137928 and HD 159834 have abundance characteristics similar to marginal Am-type stars. We also compared their patterns with the marginal Am HD 185658 (KIC 9349245) from Trust et al. (2021). The chemical element distributions of HD 2924 and the giant HD 26553 are consistent with the pattern of normal A-type stars.

Table 4. Atmospheric parameters from spectroscopic analysis.

Star name	$T_{\rm eff}$ [K]	log g [dex]	[Fe/H] [dex]	ξ [km s^{-1}]	$V_{\rm helio}$ [km s^{-1}]	v sin i [km s^{-1}]
HD 2924	8650 ± 150	3.70 ± 0.10	0.12 ± 0.18	2.60 ± 0.5	01.90 ± 0.25	30 ± 5
HD 4321	8500 ± 150	4.00 ± 0.10	0.14 ± 0.15	3.00 ± 0.5	-07.60 ± 0.70	24 ± 4
HD 26553	8350 ± 150	2.20 ± 0.10	0.08 ± 0.19	1.90 ± 0.5	-22.00 ± 2.60	10 ± 2
HD 125658	8800 ± 150	4.60 ± 0.10	0.41 ± 0.10	5.00 ± 0.5	01.70 ± 0.50	26 ± 5
HD 137928	9100 ± 150	3.80 ± 0.10	0.42 ± 0.12	4.00 ± 0.5	-03.90 ± 0.40	34 ± 5
HD 154713	8350 ± 150	3.50 ± 0.10	0.18 ± 0.15	3.00 ± 0.5	-06.30 ± 0.50	39 ± 5
HD 159834	8350 ± 150	3.90 ± 0.10	0.13 ± 0.20	3.20 ± 0.5	-16.20 ± 2.00	14 ± 3

Downloaded from https://academic.oup.com/mnras/article/521/3/3699/7069350 by ANKARA UNIVERSITY user on 04 June 2023

Table 5. Derived elemental abundances with the total error estimates of HD 2924 and HD 26553.

Atomic Sp.	HD 2924 log ϵ	HD 2924 [x/H]	HD 26553 log ϵ	HD 26553 [x/H]	Solar log $\epsilon_\odot$
C I	8.45	-0.07 ± 0.11 (6)	8.37	-0.15 ± 0.12 (19)	8.52
N I	8.05	0.13 ± 0.04 (1)	8.20	0.28 ± 0.09 (2)	7.92
O I	8.95	0.12 ± 0.04 (1)	8.91	0.08 ± 0.04 (8)	8.83
Na I	...	...	6.54	0.21 ± 0.17 (3)	6.33
Mg I	7.55	-0.03 ± 0.22 (4)	7.77	0.19 ± 0.19 (4)	7.58
Mg II	7.62	0.04 ± 0.14 (1)	7.80	0.22 ± 0.26 (2)	7.58
Al II	...	...	6.72	0.25 ± 0.05 (1)	6.47
Si I	...	...	7.68	0.13 ± 0.15 (8)	7.55
Si II	7.48	-0.07 ± 0.14 (2)	7.50	-0.05 ± 0.12 (2)	7.55
S I	...	...	7.55	0.22 ± 0.15(6)	7.33
K I	...	...	5.33	0.21 ± 0.18(1)	5.12
Ca I	6.49	0.13 ± 0.19 (7)	6.40	0.04 ± 0.24 (17)	6.36
Ca II	...	...	6.37	0.01 ± 0.13 (4)	6.36
Sc II^{HFS}	3.09	-0.08 ± 0.16 (3)	3.04	-0.13 ± 0.21 (11)	3.17
Ti I	...	...	5.01	-0.01 ± 0.20 (4)	5.02
Ti II	5.31	0.29 ± 0.26 (1)	4.99	-0.03 ± 0.19 (38)	5.02
V II^{HFS}	4.17	0.17 ± 0.22 (1)	4.02	0.02 ± 0.15 (9)	4.00
Cr I	5.76	0.09 ± 0.26 (2)	5.72	0.05 ± 0.19(9)	5.67
Cr II	5.85	0.18 ± 0.16 (10)	5.71	0.04 ± 0.17(39)	5.67
Mn I^{HFS}	5.30	-0.09 ± 0.16 (1)	5.29	-0.10 ± 0.19(8)	5.39
Mn II^{HFS}	5.30	-0.09 ± 0.04 (1)	5.26	-0.13 ± 0.07(7)	5.39
Fe I	7.62	0.12 ± 0.18 (42)	7.58	0.08 ± 0.19(202)	7.50
Fe II	7.64	0.14 ± 0.18 (46)	7.58	0.08 ± 0.11(102)	7.50
Co II	...	...	5.15	0.23 ± 0.06(1)	4.92
Ni I	...	...	6.19	-0.06 ± 0.17(20)	6.25
Ni II	...	...	6.20	-0.05 ± 0.06(3)	6.25
Cu I	...	...	4.53	0.32 ± 0.16(1)	4.21
Zn I	4.83	0.23 ± 0.13 (1)	4.70	0.10 ± 0.17(2)	4.60
Sr II	3.31	0.34 ± 0.37 (2)	3.44	0.47 ± 0.37(3)	2.97
Y II^{HFS}	2.62	0.38 ± 0.15 (1)	2.37	0.13 ± 0.17(5)	2.24
Zr II	3.21	0.61 ± 0.32 (1)	2.75	0.15 ± 0.15(8)	2.60
Ba II^{HFS}	2.41	0.28 ± 0.24 (1)	2.43	0.30 ± 0.34(4)	2.13
La II	...	...	1.61	0.44 ± 025(2)	1.17
Ce II	...	...	1.72	0.14 ± 0.18(1)	1.58

4 EVOLUTIONARY STATUS

To estimate the evolutionary status of the target stars, we pinpointed their positions precisely on the HR diagram given in Fig. 5. This is of particular importance, as it allowed us to investigate the region occupied by Am stars. With the help of isochrones and evolutionary tracks with solar metallicity (Bressan et al. 2012), we estimated the stellar masses and ages. The luminosity ($L/L_\odot$) was calculated using the standard technique. We obtained $E(B-V)$ from the work of Kervella et al. (2019) and computed extinction with the standard extinction law,

$$A_V = 3.1 \times E(B-V). \quad (3)$$

The bolometric correction (BC) was calculated using the temperature-dependent function of Torres (2010). The absolute magnitudes (M_V) were determined using *Gaia* parallaxes (Gaia Collaboration 2020). The errors in luminosities are from uncertainties in $T_{\rm eff}$, V-band indices, and *Gaia* parallaxes. Using the Stefan–Boltzmann law as in Montambaux (2018), we calculated the radius from the $T_{\rm eff}$ and log ($L/L_\odot$) values. The $E(B-V)$ values and calculated parameters are listed in Table 7. The masses, ages, and radii determined are listed in Table 8.

5 RESULTS

5.1 Normal A-type stars

5.1.1 HD 2924

This star was classified as spectral type A2IV (Cowley et al. 1969). Zorec & Royer (2012) measured $T_{\rm eff}$ as 8730 K (log $T_{\rm eff}$ = 3.941) and reported log ($L/L_\odot$) = 2.3083, mass = 3.06 $M_\odot$, and rotational velocity = 30 km s^{-1}. McDonald, Zijlstra & Boyer (2012) measured $T_{\rm eff}$ as 7800 K and reported a luminosity of 134.59 (log($L/L_\odot$) = 2.129). Duflot et al. (1995) measured a radial velocity of 1.9 km s^{-1}, whereas de Bruijne & Eilers (2012) and Brandt (2021) reported a radial velocity of 2.1 km s^{-1}. In this study, we measured the fundamental parameters of HD 2924 as $T_{\rm eff}$ = 8650 K, log g = 3.7, and ξ = 2.60 km s^{-1}. We derived v sin i and $V_{\rm helio}$ as 30 and 1.90 km s^{-1}, respectively. The abundance of calcium is 0.13 dex and that of scandium -0.08 dex. The iron-peak and heavy elements do not show significant overabundance, as we would expect for Am stars, hence we classified HD 2924 as a normal A-type star. The elemental abundance distribution of HD 2924 is shown in Fig. 2. We estimated the mass, age, and radius as 2.40 ± 0.09 $M_\odot$, 490 ± 60 Myr, and 4.20 ± 0.40 $R_\odot$, respectively. The difference between the calculated luminosity in this study and the luminosity given in Zorec & Royer (2012) is due largely to the parallax values used in the calculation of luminosities.

Downloaded from https://academic.oup.com/mnras/article/521/3/3699/7069350 by ANKARA UNIVERSITY user on 04 June 2023

Table 6. Derived elemental abundances with the total error estimates of HD 4321, HD 125658, HD 137928, HD 154713, and HD 159834.

Atomic sp.	HD 4321 log ϵ	HD 4321 [x/H]	HD 125658 log ϵ	HD 125658 [x/H]	HD 137928 log ϵ	HD 137928 [x/H]	HD 154713 log ϵ	HD 154713 [x/H]	HD 159834 log ϵ	HD 159834 [x/H]	Solar log $\epsilon_\odot$
C I	8.72	0.20 ± 0.07 (11)	8.72	0.20 ± 0.09(7)	8.73	0.21 ± 0.08(2)	8.42	-0.10 ± 0.11(3)	8.46	-0.06 ± 0.08(11)	8.52
O I	8.88	0.05 ± 0.25 (1)	8.58	-0.25 ± 0.18(2)	9.03	0.20 ± 0.01(1)	...	...	8.72	-0.11 ± 0.05(1)	8.83
Na I	6.73	0.40 ± 0.12 (3)	6.71	0.38 ± 0.10(2)	...	...	...	...	6.40	0.07 ± 0.14(2)	6.33
Mg I	7.57	-0.01 ± 0.15 (4)	7.73	0.15 ± 0.14(3)	7.78	0.20 ± 0.21(4)	7.25	-0.19 ± 0.22(4)	7.49	-0.09 ± 0.13(4)	7.58
Mg II	...	...	...	...	...	...	...	...	7.62	0.04 ± 0.10(2)	7.58
Al II	...	...	6.70	0.23 ± 0.03(1)	...	...	...	...	...	...	6.47
Si I	7.63	0.08 ± 0.14 (3)	7.98	0.43 ± 0.12(7)	...	...	...	...	7.75	0.20 ± 0.11(5)	7.55
Si II	7.56	0.01 ± 0.18 (1)	...	...	7.77	0.22 ± 0.17(3)	7.43	-0.12 ± 0.17(3)	...	...	7.55
S I	7.66	0.33 ± 0.12 (5)	7.71	0.38 ± 0.11(2)	7.69	0.36 ± 0.10(1)	7.64	0.31 ± 0.10(1)	7.41	0.08 ± 0.09(1)	7.33
K I	...	...	...	...	...	...	...	...	5.13	0.01 ± 0.13(1)	5.12
Ca I	6.20	-0.16 ± 0.16 (10)	6.25	-0.11 ± 0.15(11)	6.47	0.11 ± 0.16(3)	6.05	-0.31 ± 0.18(6)	6.28	-0.08 ± 0.17(12)	6.36
Ca II	6.31	-0.05 ± 0.05 (2)	6.27	-0.09 ± 0.04(2)	...	...	...	...	...	...	6.36
Sc II^{HFS}	2.62	-0.55 ± 0.14 (5)	2.76	-0.41 ± 0.18(3)	2.79	-0.38 ± 0.19(2)	2.63	-0.54 ± 0.11(2)	2.86	-0.27 ± 0.12(5)	3.17
Ti II	5.23	0.21 ± 0.22 (18)	5.39	0.37 ± 0.10(17)	5.31	0.29 ± 0.18(11)	5.21	0.19 ± 0.23(11)	5.39	0.37 ± 0.22(22)	5.02
V II^{HFS}	4.18	0.18 ± 0.12 (2)	4.42	0.42 ± 0.08(2)	4.52	0.52 ± 0.13(1)	4.21	0.21 ± 0.11(1)	4.31	0.31 ± 0.12(3)	4.00
Cr I	5.84	0.17 ± 0.15 (5)	6.17	0.50 ± 0.15(3)	...	...	5.79	0.12 ± 0.27(2)	...	...	5.67
Cr II	5.87	0.20 ± 0.11 (24)	6.07	0.40 ± 0.07(19)	6.15	0.48 ± 0.12(18)	5.83	0.16 ± 0.25(5)	5.86	0.19 ± 0.12(21)	5.67
Mn I^{HFS}	5.62	0.23 ± 0.18 (2)	5.91	0.32 ± 0.13(4)	5.81	0.42 ± 0.15(3)	5.58	0.19 ± 0.16(1)	5.60	0.21 ± 0.13(3)	5.39
Mn II^{HFS}	5.61	0.22 ± 0.03 (1)	5.98	0.39 ± 0.08(2)	...	...	...	...	...	...	5.39
Fe I	7.64	0.14 ± 0.15 (106)	7.93	0.43 ± 0.13(129)	7.92	0.42 ± 0.15(64)	7.68	0.18 ± 0.20(59)	7.66	0.16 ± 0.16(108)	7.50
Fe II	7.62	0.12 ± 0.15 (49)	7.89	0.39 ± 0.08(50)	7.91	0.41 ± 0.14(40)	7.68	0.18 ± 0.21(36)	7.65	0.15 ± 0.16(59)	7.50
Ni I	6.46	0.21 ± 0.14 (6)	6.95	0.70 ± 0.12(13)	6.90	0.65 ± 0.13(4)	6.47	0.22 ± 0.15(6)	6.55	0.30 ± 0.13(10)	6.25
Cu I	...	...	4.93	0.72 ± 0.13(1)	...	...	...	...	4.53	0.32 ± 0.21(2)	4.21
Zn I	5.08	0.48 ± 0.14 (2)	5.31	0.71 ± 0.12(2)	5.38	0.78 ± 0.13(1)	4.79	0.19 ± 0.14(1)	5.05	0.45 ± 0.17(2)	4.60
Sr II	3.59	0.62 ± 0.39 (2)	3.46	0.49 ± 0.47(1)	3.67	0.70 ± 0.51(1)	3.82	0.85 ± 0.48(1)	3.94	0.97 ± 0.51(1)	2.97
Y II^{HFS}	2.56	0.32 ± 0.11 (2)	3.51	1.07 ± 0.10(5)	3.26	1.02 ± 0.15(3)	...	...	2.81	0.57 ± 0.17(7)	2.24
Zr II	3.23	0.63 ± 0.14 (2)	4.08	1.48 ± 0.13(3)	3.81	1.21 ± 0.11(3)	3.28	0.68 ± 0.18(2)	3.51	0.91 ± 0.10(3)	2.60
Ba II^{HFS}	3.06	0.83 ± 0.27 (3)	3.61	1.18 ± 0.23(3)	3.36	1.23 ± 0.22(2)	2.92	0.79 ± 0.29(3)	3.02	0.89 ± 0.30(2)	2.13
La II	2.45	1.28 ± 0.14 (1)	2.58	1.41 ± 0.12(1)	...	...	...	...	2.68	1.51 ± 0.19(1)	1.17
Ce II	1.94	0.36 ± 0.12 (1)	2.99	1.41 ± 0.11(1)	...	...	...	...	2.77	1.19 ± 0.15(4)	1.58
Nd II	2.55	1.05 ± 0.20 (2)	...	...	...	...	...	...	...	...	1.50
Sm II	2.97	1.96 ± 0.14 (1)	...	...	...	...	...	...	2.59	1.58 ± 0.13(1)	1.01
Eu II	...	...	...	...	...	...	...	...	1.42	0.91 ± 0.14(1)	0.51
Gd II	2.90	1.78 ± 0.10 (1)	...	...	...	...	...	...	...	...	1.12

Downloaded from https://academic.oup.com/mnras/article/521/3/3699/7069350 by ANKARA UNIVERSITY user on 04 June 2023

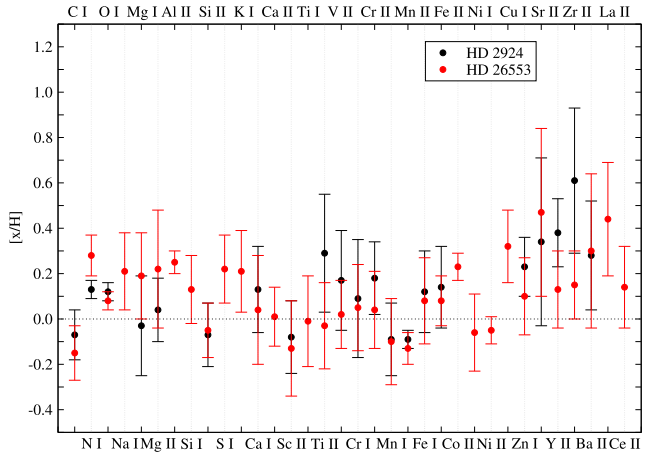


Figure 2. The differences between our derived chemical abundances and the solar abundances found by Grevesse & Sauval (1998) for HD 2924 and HD 26553.

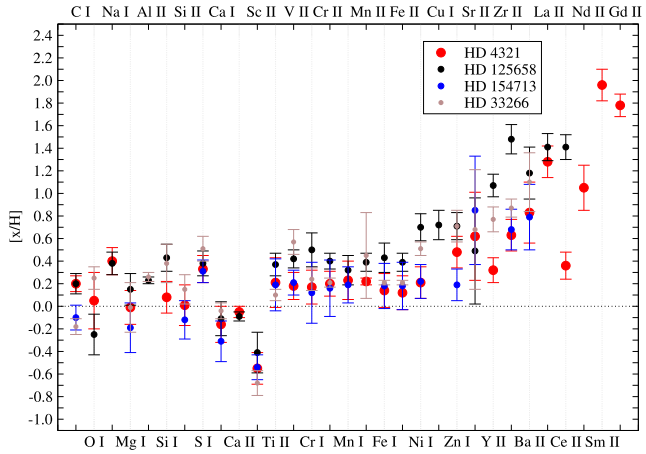


Figure 3. The differences between our derived chemical abundances and the solar abundances found by Grevesse & Sauval (1998) for the classic Am stars HD 4321, HD 125658, and HD 154713. HD 33266 is a classical Am star studied by Çalışkan et al. (2015).

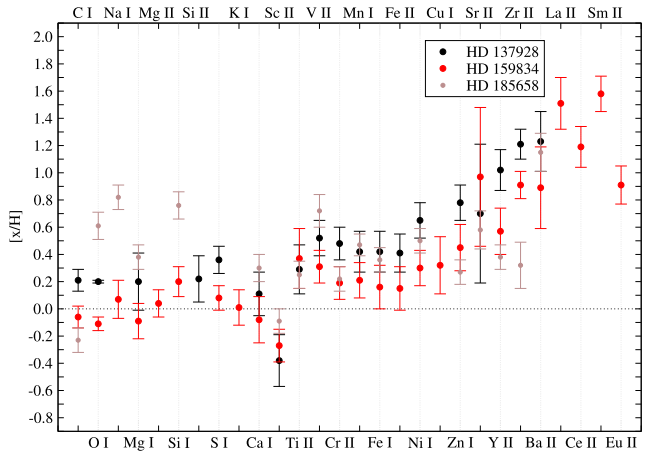


Figure 4. The differences between our derived chemical abundances and the solar abundances found by Grevesse & Sauval (1998) for the marginal Am stars HD 137928 and HD 159834. HD 185658 is a marginal Am star studied by Trust et al. (2021).

5.1.2 HD 26553

HD 26553 was listed as A4III by Cowley et al. (1969). de Bruijne & Eilers (2012) and Brandt (2021) reported a radial velocity of -24.9 km s^{-1}. Royer et al. (2002) measured v sin i as 18 km s^{-1}. We determined the atmospheric parameters of HD 26553 as follows: $T_{\rm eff}$ = 8350 K, log g = 2.2, and ξ = 1.9 km s^{-1}. We measured v sin i and $V_{\rm helio}$ as 12 and 22 km s^{-1}, respectively. With [Ca/H] = 0.04 dex, [Sc/H] = -0.13 dex, and an average abundance of iron-peak and heavy elements, the star exhibits solar-like abundances. The chemical abundance pattern, shown in Fig. 2, does not show Am characteristics and is consistent with the pattern of normal A-type stars. The physical parameters were estimated as mass = 5.1 ± 0.3 M$_\odot$, age = 90 ± 5 Myr, and radius = 20.3 ± 2.2 R$_\odot$. The HR diagram reveals that HD 26553 is a post-terminal-age main sequence (TAMS) star.

5.2 Classical Am stars

5.2.1 HD 4321

HD 4321 was listed as an A2III star in the HD catalogue of Cannon & Pickering (1993). The star's radial velocity was measured as -8.3 km s^{-1} (de Bruijne & Eilers 2012; Brandt 2021). McDonald et al. (2012) reported an effective temperature of 7787 K and a luminosity of 50.05 L$_\odot$ (log (L/L$_\odot$) = 1.70). Royer et al. (2002) measured v sin i as 24 km s^{-1}. We measured the star's $T_{\rm eff}$, log g, and ξ as 8500 K, 4.00, and 3.00 km s^{-1}, respectively. We measured the v sin i and $V_{\rm helio}$ of HD 4321 as 24 and -7.6 km s^{-1}. Its [Ca/H] and [Sc/H] values were found to be underabundant with respect to the solar abundances by -0.16 and -0.55 dex, respectively. The star exhibits an overabundance (on average) in iron-peak and rare-earth elements with respect to the solar abundances. Its chemical abundance pattern, shown in Fig. 3, implies a classical Am star. The mass of HD 4321 was estimated as 2.00 ± 0.08 M$_\odot$. We estimated the age and radius as 625 ± 60 Myr and 3.40 ± 0.30 R$_\odot$, respectively.

5.2.2 HD 125658

This target was first noted as an Am-type candidate by Bertaud (1958). Cowley et al. (1969) classified HD 125658 as A5III. It was listed as an A2 star in the HD catalogue (Cannon & Pickering 1993). de Bruijne & Eilers (2012) and Brandt (2021) measured the radial velocity as 1.3 km s^{-1}. McDonald et al. (2012) derived $T_{\rm eff}$ as 8123 K and the luminosity as 17.9 L$_\odot$ (log (L/L$_\odot$) = 1.25). David & Hillenbrand (2015) reported $T_{\rm eff}$ as 8430 K, log g as 4.27, the mean age from 1D posterior as 581 Myr, and the mass as 1.9 M$_\odot$. From 2D linear interpolation, the age and mass were measured as 363 Myr and 1.78 M$_\odot$, respectively. Royer et al. (2002) measured a v sin i of 26 km s^{-1}. We measured the atmospheric parameters of HD 125658 as $T_{\rm eff}$ = 8800 K, log g = 4.60, and ξ = 5.07 km s^{-1}. Its v sin i and heliocentric radial velocity $V_{\rm helio}$ were derived as 26 and 1.66 km s^{-1}. HD 125658 has characteristic abundances consistent with the abundance of classical Am-type stars. The underabundance of Ca at -0.11 and Sc at -0.41 and the overabundance pattern in iron-peak and heavy elements with respect to the solar abundances are shown in Fig. 3. We note that the star has significantly higher iron, nickel, copper, and zinc abundances than the other two Am-type samples. The mass, age, and radius were estimated as 1.75 ± 0.06 M$_\odot$, 370 ± 40 Myr, and 1.80 ± 0.20 R$_\odot$, respectively.

Downloaded from https://academic.oup.com/mnras/article/521/3/3699/7069350 by ANKARA UNIVERSITY user on 04 June 2023

Table 7. The logarithmic effective temperature log $T_{\rm eff}$ (this study), $E(B-V)$ (Kervella et al. 2019), bolometric correction BC (Torres 2010), absolute magnitude M_V (this study), parallax π (Gaia Collaboration 2020), and luminosity log(L/L$_\odot$) (this study).

Star name	log $T_{\rm eff}$	π (mas)	$E(B-V)$	BC	M$_V$	log(L/L$_\odot$)
HD 2924	3.9370 [0.0075]	4.3978 [0.0292]	0.040	−0.0156	−0.2078	1.9453 [0.0100]
HD 4321	3.9294 [0.0076]	5.9672 [0.0209]	0.034	−0.0001	0.2834	1.7427 [0.0078]
HD 26553	3.9217 [0.0077]]	1.5391 [0.0370]	0.170	0.0120	−3.5107	3.2555 [0.0215]
HD 125658	3.9445 [0.0072]	11.9629 [0.1441]	0.007	−0.0341	1.6918	1.1929 [0.0147]
HD 137928	3.9590 [0.0071]	8.1997 [0.0243]	0.014	−0.0341	0.9556	1.5051 [0.0111]
HD 154713	3.9217 [0.0077]	6.3445 [0.0227]	0.021	0.0120	0.3878	1.6961 [0.0070]
HD 159834	3.9217 [0.0077]	6.4269 [0.1041]	0.023	0.0120	0.0687	1.8237 [0.0153]

Table 8. The masses, ages, and radii of the target stars.

Star name	Mass [M$_\odot$]	Age [Myr]	Radius [R$_\odot$]
HD 2924	2.40 [0.09]	490 [40]	04.20 [0.40]
HD 4321	2.00 [0.08]	625 [50]	03.40 [0.30]
HD 26553	5.10 [0.30]	090 [05]	20.30 [2.20]
HD 125658	1.75 [0.06]	370 [40]	01.80 [0.20]
HD 137928	2.00 [0.07]	550 [50]	02.30 [0.25]
HD 154713	2.00 [0.08]	675 [60]	03.40 [0.30]
HD 159834	2.20 [0.07]	600 [50]	03.90 [0.40]

5.2.3 HD 154713

HD 154713 was listed as an A0 star in the HD catalogue (Cannon & Pickering 1993). The spectral type of HD 154713 was classified as A3IV (Cowley et al. 1969). Zorec & Royer (2012) measured $T_{\rm eff}$ as 8550 K (log $T_{\rm eff}$ = 3.932) and reported log (L/L$_\odot$) = 1.81, mass = 2.52 M$_\odot$, and a rotational velocity of 39 km s^{-1}. McDonald et al. (2012) measured $T_{\rm eff}$ as 7954 K and reported a luminosity of 47.48 L$_\odot$ (log (L/L$_\odot$) = 1.679). de Bruijne & Eilers (2012) and Brandt (2021) reported a radial velocity of −8.7 km s^{-1}. We determined the atmospheric parameters of HD 154713 as $T_{\rm eff}$ = 8350 K, log g = 3.50, and ξ = 3.00 km s^{-1}. We derived the values of v sin i and $V_{\rm helio}$ as 39 and −6.30 km s^{-1}, respectively. The abundance of calcium is −0.31 dex and that of scandium −0.54 dex. The iron-peak and heavy element abundances are slightly overabundant with respect to solar; hence, HD 154713 is consistent with classical Am-type stars. The abundance pattern is shown in Fig. 3. We estimated the mass, age, and radius as 2.00 ± 0.08 M$_\odot$, 675 ± 60 Myr, and 3.40 ± 0.40 R$_\odot$, respectively.

5.3 Marginal Am stars

5.3.1 HD 137928

This star was ascribed a spectral type A2 IV (Cowley et al. 1969). Zorec & Royer (2012) measured $T_{\rm eff}$ as 8649 K (log $T_{\rm eff}$ = 3.937) and reported log (L/L$_\odot$) = 1.744, mass = 2.45 M$_\odot$, and v sin i = 34 km s^{-1}. McDonald et al. (2012) measured $T_{\rm eff}$ as 8637 K and reported a luminosity of 32.62 L$_\odot$ (log (L/L$_\odot$) = 1.513). de Bruijne & Eilers (2012) and Brandt (2021) reported a radial velocity of −4.90 km s^{-1}. Kervella et al. (2019) measured the radial velocity as −4.985 km s^{-1}. We determined the $T_{\rm eff}$ of HD 137928 as 9100 K and log g and ξ were measured as 3.8 and 4.03 km s^{-1}, respectively. The v sin i was determined as 34 km s^{-1} and $V_{\rm helio}$ as −3.9 km s^{-1}. The abundance of calcium is 0.11 dex and that of scandium is −0.38 dex. The Ca abundance is nearly solar-like, while Sc is slightly underabundant. Iron-peak and heavy elements have an over-abundance, implying marginal Am star abundance characteristics.

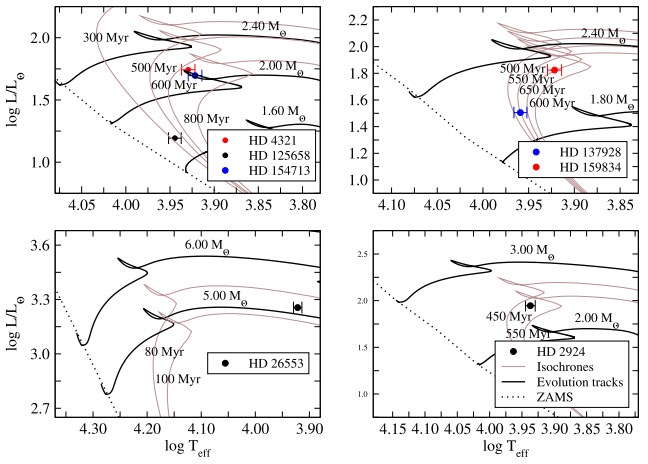


Figure 5. The position of target stars on the HR diagram. Evolutionary tracks and isochrones are from Bressan et al. (2012).

HD 137928 has high iron, nickel, and zinc abundances. This makes it a metal-rich star. The elemental abundance pattern of HD 137928 is shown in Fig. 4. Its mass was determined as 2.00 ± 0.07 M$_\odot$. HD 137928's radius was measured as 2.30 ± 0.25 R$_\odot$ at the age of 550 ± 50 Myr.

5.3.2 HD 159834

This star was first classified as A7III by Eggen (1962). Cowley et al. (1969) reported the spectral type as A7IV. HD 159834 was listed as an A2 star in the HD catalogue (Cannon & Pickering 1993). Zorec & Royer (2012) measured its $T_{\rm eff}$ as 7925 K (log $T_{\rm eff}$ = 3.899) and reported a luminosity of log (L/L$_\odot$) = 1.6256, a mass of 2.29 M$_\odot$, and a rotational velocity of 19 km s^{-1}. McDonald et al. (2012) measured $T_{\rm eff}$ as 7724 K and reported a luminosity of 34.94 L$_\odot$ (log (L/L$_\odot$) = 1.54). de Bruijne & Eilers (2012) and Brandt (2021) reported a radial velocity of −17 km s^{-1}. Burkhart & Coupry (1991) measured $T_{\rm eff}$, log g, and [Fe/H] as 8030 K, 3.7, and 0.1 dex, respectively. Kervella et al. (2019) measured a radial velocity of −16.82 km s^{-1}. Finally, the atmospheric parameters of HD 159834 were determined as $T_{\rm eff}$ = 8350 K, log g = 3.9, and ξ = 3.2 km s^{-1}. We measured v sin i and $V_{\rm helio}$ as 14 and −16.20 km s^{-1}. The calcium abundance is −0.08 dex, while that of scandium is −0.27 dex. The abundances are close to solar, with scandium slightly underabundant. The iron-peak and heavy elements are moderately overabundant, implying a marginal Am star. The elemental abundance pattern is shown in Fig. 4. We determined the mass, age, and radius as 2.20 ± 0.07 M$_\odot$, 600 ± 50 Myr, and 3.90 ± 0.4 R$_\odot$, respectively.

Downloaded from https://academic.oup.com/mnras/article/521/3/3699/7069350 by ANKARA UNIVERSITY user on 04 June 2023

6 CONCLUSION

In this work, we present a chemical abundance analysis of seven A-type stars, for which detailed abundance analyses are absent in the literature, to search for their chemical anomalies. These stars are slow-rotating A-type stars. Slow rotators were targeted because rotational velocity is linked to the mixing process of stellar materials that suppress the effect of chemical separation. We first obtained fundamental atmospheric parameters and velocities for each target, including the effective temperature ($T_{\rm eff}$), surface gravity (log g), metallicity [Fe/H], microturbulent velocity (ξ), rotational velocity (v sin i), and radial velocity ($V_{\rm helio}$). We then performed a detailed abundance analysis for each star, obtained its luminosity log ($L/L_{\odot}$), and pinpointed its position in the HR diagram. Using evolutionary tracks and isochrones, we estimated the masses and ages of the targets. Using the $T_{\rm eff}$ and luminosity values, we calculated the radii of the stars. The present work is the first detailed abundance analysis of these targets. Six of the targets are main-sequence stars, with some of them near to the TAMS, while HD 26553 was revealed to be a post-TAMS giant. Based on the spectral analysis, the resulting chemical abundance patterns of five targets revealed that they are Am-type stars, with HD 4321, HD 125658, and HD 154713 classified as classical Am stars, while HD 137928 and HD 159834 were classified as marginal Am stars. The abundance patterns of HD 2924 and HD 26553 are consistent with those of normal A-type stars. Two of our samples, HD 125658 (classified as a classical Am star) and HD 137928 (classified as a marginal Am star), have high iron, nickel, and zinc abundances. Their carbon, sodium, magnesium, sulphur, scandium, vanadium, manganese, yttrium, and barium abundances are very similar. They also have very similar atmospheric and physical parameters. Considering all these similarities, these two stars are among the most metal-rich Am stars. The HR diagram shows that Am stars populate the main sequence. On average, based on chemical separation theory, the main-sequence slow rotator HD 2924 is expected to exhibit Am characteristics. The presence of its non-Am characteristics poses a challenge to the rotation effect on the hypothesized chemical separation, which shows that there is a need to study more such targets to explore the origin of their peculiarity and their interior processes.

ACKNOWLEDGEMENTS

The authors acknowledge the TÜBİTAK National Observatory (TUG) with the project ID 14BRTT150-671.

DATA AVAILABILITY

The data underlying this article are available in the article and in its online supplementary material. Upon request, further data underlying this article will be shared on reasonable request to the corresponding author.

REFERENCES

Abt H. A., 2000, ApJ, 544, 933
Abt H. A., 2009, PASP, 121, 1291
Abt H. A., Morgan W. W., 1976, ApJ, 205, 446
Abt H. A., Moyd K. I., 1973, ApJ, 182, 809
Adelman S. J., Unsuree N., 2007, Baltic Astron., 16, 183
Bertaud C., 1958, Journal des Observateurs, 42, 45
Brandt T. D., 2021, ApJS, 254, 42
Bressan A., Marigo P., Girardi L., Salasnich B., Dal Cero C., Rubele S., Nanni A., 2012, MNRAS, 427, 127
Burkhart C., Coupry M. F., 1991, A&A, 249, 205
Çalışkan Ş., Kılıçoğlu T., Elmaslı A., Nasolo Y., Avcı Z., Albayrak B., 2015, New Astron., 34, 6
Cannon A. J., Pickering E. C., 1993, Harv. Ann., 91-100, 1918
Cowley A., Cowley C., Jaschek M., Jaschek C., 1969, AJ, 74, 375
David T. J., Hillenbrand L. A., 2015, ApJ, 804, 146
de Bruijne J. H. J., Eilers A. C., 2012, A&A, 546, A61
Duflot M., Fehrenbach C., Mannone C., Burnage R., Genty V., 1995, A&AS, 110, 177
Eggen O. J., 1962, Royal Greenwich Observatory Bulletins, 51, 79
Fossati L., Bagnulo S., Landstreet J., Wade G., Kochukhov O., Monier R., Weiss W., Gebran M., 2008, A&A, 483, 891
Frebel A., Casey A. R., Jacobson H. R., Yu Q., 2013, ApJ, 769, 57
Gaia Collaboration, 2020, A&A, 649A, 1G
Grevesse N., Sauval A. J., 1998, Space Sci. Rev., 85, 161
Kervella P., Arenou F., Mignard F., Thévenin F., 2019, A&A, 623, A72
Khokhlova V. L., 1981, in Chemically peculiar stars of the upper main sequence; International Conference on Astrophysics, 23rd, Liege, Belgium, June 23-26, 1981, Reports. (A82-37717 18-39) Liege. Universite de Liege, p. 457
Kochukhov O., 2018, BinMag: Widget for comparing stellar observed with theoretical spectra, Astrophysics Source Code Library, record ascl:1805.015
Kupka F., Piskunov N., Ryabchikova T. A., Stempels H. C., Weiss W. W., 1999, A&AS, 138, 119
Kurucz R., 1993a, TLAS9 Stellar Atmosphere Programs and 2 km/s grid. Kurucz CD-ROM No. 13. Smithsonian Astrophysical Observatory, Cambridge, Mass
Kurucz R., 1993b, SYNTHE Spectrum Synthesis Programs and Line Data, Kurucz CD-ROM No. 18. Cambridge
Kurucz R. L., 2005a, Mem. Soc. Astron. Ital. Suppl., 8, 14
Kurucz R. L., 2005b, Mem. Soc. Astron. Ital. Suppl., 8, 189
Kurucz R. L., Bell B., 1995, Atomic line list, Kurucz CD-ROM. Smithsonian Astrophysical Observatory, Cambridge, MA
McDonald I., Zijlstra A. A., Boyer M. L., 2012, MNRAS, 427, 343
Michaud G., 1982, ApJ, 258, 349
Michaud G., Alecian G., Richer J., 2015, Atomic Diffusion in Stars, Astronomy and Astrophysics Library. Springer International Publishing, Switzerland
Monier R., 2019, Res. Notes Am. Astron. Soc., 3, 167
Montambaux G., 2018, Foundations of Physics, 48, 395
Napiwotzki R., Schoenberner D., Wenske V., 1993, A&A, 268, 653
Oja T., 1991, A&AS, 89, 415
Paunzen E., 2015, A&A, 580, A23
Piskunov N. E., Kupka F., Ryabchikova T. A., Weiss W. W., Jeffery C. S., 1995, A&AS, 112, 525
Preston G. W., 1974, ARA&A, 12, 257
Roman N. G., Morgan W. W., Eggen O. J., 1948, ApJ, 107, 107
Royer F., Grenier S., Baylac M. O., Gómez A. E., Zorec J., 2002, A&A, 393, 897
Ryabchikova T. A., Piskunov N. E., Stempels H. C., Kupka F., Weiss W. W., 1999, Phys. Scripta Vol. T, 83, 162
Sbordone L., Bonifacio P., Castelli F., Kurucz R. L., 2004, Mem. Soc. Astron. Ital. Suppl., 5, 93
Takeda Y., Han I.-W., Kang D.-I., Lee B.-C., Kim K.-M., 2008, J. Korean Astron. Soc., 41, 83
Titus J., Morgan W. W., 1940, ApJ, 92, 256
Torres G., 2010, AJ, 140, 1158
Trust O., Jurua E., De Cat P., Joshi S., Lampens P., 2021, MNRAS, 504, 5528
Zorec J., Royer F., 2012, A&A, 537, A120

Downloaded from https://academic.oup.com/mnras/article/521/3/3699/7069350 by ANKARA UNIVERSITY user on 04 June 2023

SUPPORTING INFORMATION

Supplementary data are available at *MNRAS* online.

Table 2. List of spectral lines used in the abundance analysis of target stars.

Please note: Oxford University Press is not responsible for the content or functionality of any supporting materials supplied by the authors. Any queries (other than missing material) should be directed to the corresponding author for the article.

This paper has been typeset from a TEX/LATEX file prepared by the author.

Downloaded from https://academic.oup.com/mnras/article/521/3/3699/7069350 by ANKARA UNIVERSITY user on 04 June 2023